ELSEVIER

Powder Technology 121 (2001) 106–115

POWDER TECHNOLOGY

www.elsevier.com/locate/powtec

Continuous cooling crystallization from solution

Håkan Gros [a,*], Teuvo Kilpiö [b], Juha Nurmi [c]

[a] *Cultor Food Science, Xyrofin Division, 02460 Kantvik, Finland*
[b] *Cultor Food Science Technology Development, 02460 Kantvik, Finland*
[c] *Cultor Food Science Technology Development, 02460 Kantvik, Finland*

Abstract

In this paper, a model was constructed in order to simulate the behaviour of slow growing crystals in high viscosity systems in a tower crystallizer. This type of crystallizer, ideally, is an application of the plug–flow concept. Plug–flow conditions are an advantage when a narrow crystal size distribution is the goal desired. The model was based on the following assumptions: steady state operation, no nucleation or growth rate dispersion, no breakage, size-dependent growth and settling of crystals. A simulation example for sucrose is presented although the model applies to other similar systems.

Keywords: Theoretical methods; Continuous crystallization; Plug–flow; Sucrose; Settling; Simulation

1. Introduction

There is a wealth of equipment variations that face the practitioner having the task of creating a crystallization process for a specific product. In chemical engineering, development has been towards continuous processes, and crystallization is no exception. The often cited advantages for continuous operations, compared to batch operations, is better trimming to optimal conditions, less down time and a smaller size of crystallizers and tankage. In crystallization, these advantages must be balanced against specific drawbacks, such as the slow attainment of steady state, potential instability of operation and incrustation problems.

The classification of crystallizers is often made based on the way of effecting supersaturation (evaporation, cooling, salting-out, etc.). When discussing continuous crystallization, standard textbooks usually present the MSMPR (Mixed Suspension Mixed Product Removal, Forced circulation) crystallizer, the DTB (draft tube baffle) and the Krystal crystallizer and variations of these. Many of them can be operated either as cooling crystallizers or evaporative crystallizers. A common feature for these, however, is that they are predominantly intended for rapid crystallization of inorganic products. A cursory perusal of some standard books [1–4] shows that no equipment classification, based on crystal growth rate and/or mother liquor viscosity, is attempted. Moreover, the application of crystallization theory to calculate crystal size distributions and yields is very much focused on MSMPR and the like. Nevertheless, it seems to the authors of this article that crystal growth rate and viscosity are at least as relevant criteria as supersaturation.

Sugar is one of the largest industries in the world, and crystallization is of central importance there. In order to get insight into crystallization of slow growing and/or high viscosity systems, one needs to go to the more specialized literature. Low-grade sugar recovery has traditionally been carried out in horizontal cooling crystallizers. In the 1970s, the first attempts to use vertical crystallization towers were made, and nowadays, these have become fairly common in both the sugar and related industries [5–7].

The intention of this paper to explore the advantages of using tower-type vertical crystallizers for crystallization in medium to high viscosity systems with slow crystallization kinetics. Compared to other configurations, this crystallizer definitely is an application of the plug–flow concept. It would seem that plug–flow conditions should be an advantage in continuous crystallization systems, where a narrow crystal size distribution is the goal. This should be true, especially for high viscosity systems, where methods that utilize, e.g. fines traps and segregation based on sedimentation do not work well.

* Corresponding author. Danisco Sugar OY, Sokeritehtaantie 20, 02460 Kantvik, Finland. Tel.: +358-405-462486; fax: +358-929-74578.
E-mail address: hakan.gros@danisco.com (H. Gros).

0032-5910/01/$ - see front matter
PII: S0032-5910(01)00382-5

2. The model for continuous cooling crystallizer

2.1. Basic assumptions of the model

Continuous crystallization with settling taking place is modeled. The model is based on the following assumptions:

- The process is in steady state, which means that (a) mass does not accumulate in the balance volume, and (b) the number of crystals entering and leaving the balance volume are equal.
- The inlet solution already contains small crystals.
- No nucleation or growth rate dispersion takes place. These assumptions are fairly rough simplifications.
- No breakage of crystals takes place.
- Plug flow conditions prevail. This assumption is discussed in Section 4.

In the first attempt to model the CSD (crystal size distribution) inside the crystallizer, a simple approach is selected. The crystallizer is of the type presented in Fig. 1. There, the feed stream arrives at the top of the crystallizer. Crystals of different sizes have different settling velocities. Therefore, their residence time inside the crystallizer is not the same. Then, the small particles remain for a longer time inside the crystallizer than the larger ones. When having co-current operation, i.e. settling in same direction as mass flow, the CSD is expected to become narrower as crystals travel down the crystallizer. The calculation is started from the top of the tower and it continues step-wise until the bottom of the tower is reached.

2.2. The model equations

The model consists of mass balance equations, expressions for physical properties, and phenomenological equations and definition equations.

2.2.1. The mass balance equations

The total mass flow remains constant and it can be calculated from initial values:

$$\dot{m}_{\mathrm{tot}} = \dot{m}_{\mathrm{cr}}(0) + \dot{m}_{\mathrm{ml}}(0) \tag{1}$$

The total mass flow of crystals after the jth step can be calculated as a sum of individual mass flows of classes of crystals:

$$\dot{m}_{\mathrm{cr}}(j) = \sum_{i=1}^{N_s} \dot{m}_{\mathrm{cr},i}(j) \tag{2}$$

The mass flow of mother liquor after the jth step can be calculated by the total mass balance:

$$\dot{m}_{\mathrm{ml}}(j) = \dot{m}_{\mathrm{tot}} - \dot{m}_{\mathrm{cr}}(j) \tag{3}$$

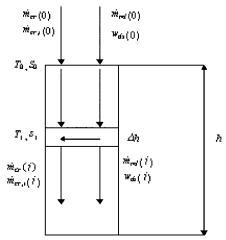

Fig. 1. A vertical continuous cooling crystallizer.

The mass fraction of dry substance in the mother liquor can then be evaluated from the dry substance balance:

$$w_{\mathrm{ds}}(j) = \left(\dot{m}_{\mathrm{cr}}(0) + \dot{m}_{\mathrm{ml}}(0)\, w_{\mathrm{ds}}(0) - \dot{m}_{\mathrm{cr}}(j)\right)/\dot{m}_{\mathrm{ml}}(j) \tag{4}$$

In this way, the formation of solid phase can be calculated from the top of the crystallizer down to the bottom.

2.2.2. Phenomenological expressions

The particles are moving due to flow with the main stream and due to settling. Settling can be described by a modified Stokes' equation for hindered settling: Stokes' equation is modified by an addition of a volume fraction dependent term, which takes into account hindered settling. It is also modified by optimizing the coefficient in the equation in order take into account the effects of nonspherical form of the particles, cf. Ditl et al. [8].

$$v_{\mathrm{set},i} = \frac{K_1(\rho_{\mathrm{cr}} - \rho_{\mathrm{ml}})\bar{L}_i^2 g(1 - x_{\mathrm{cr}})^{K_2}}{\eta_{\mathrm{ml}}} \tag{5}$$

The settling experiments were conducted by first filling the measuring cylinder with saturated solution at room temperature. Then, equal-sized crystals were added. The slow settling of the crystals could then be monitored through the upper front motion. Thus, when the particles were flowing down, some solution was moving upward in order to replace the volume fraction. After making experiments with a couple of crystal sizes, the above equation was fitted to the data by parameter estimation of the coefficients K_1 and K_2.

It now remains to present the expressions for the growth rate. The presentation is based on surface reaction and diffusion dependent growth.

The mass growth of crystals per unit surface area according to Myerson [2], p. 56 is:

$$\frac{\mathrm{d}m_{\mathrm{cr}}}{A_{\mathrm{c}}\mathrm{d}t} = K_{\mathrm{g}}\Delta C \tag{6}$$

If an assumption of first-order dependency of diffusion and surface reaction on concentration is made, the combined overall mass transfer coefficient can be calculated using the equation:

$$\frac{1}{K_{\mathrm{g}}} = \frac{1}{k_{\mathrm{d}}} + \frac{1}{k_{\mathrm{r}}} \rightarrow K_{\mathrm{g}} = \frac{k_{\mathrm{d}}k_{\mathrm{r}}}{k_{\mathrm{d}} + k_{\mathrm{r}}} \tag{7}$$

The linear growth rate can be calculated from the mass growth rate by using the expression of Mersmann [3], p. 33:

$$G = \frac{\mathrm{d}L}{\mathrm{d}t} = \frac{k_a}{3\rho_{cr}k_v}\frac{1}{A_c}\frac{\mathrm{d}m_{cr}}{\mathrm{d}t} \tag{8}$$

or combined with Eq. (7)

$$G = \frac{k_a}{3\rho_{cr}k_v}\frac{k_d k_r}{k_d + k_r}\Delta C \tag{9}$$

The concentration difference between supersaturated and saturated solution can be evaluated using the equation by Ekelhof [9], p. 64:

$$\Delta C = \frac{q_{s/w}}{q_{s/w}+1}\rho_{ml} - \frac{q_{s/w,sat}}{q_{s/w,sat}+1}\rho_{sat} \tag{10}$$

In sugar technology, it is customary to use the supersaturation coefficient, S, which according to Bubnik et al. [10], p. 207 is defined by:

$$S = \frac{w_{ds}/(1-w_{ds})}{\left[w_{ds,sat}/(1-w_{ds,sat})\right]} \tag{11}$$

The mass fraction of dry substance for a given supersaturation at known temperature can be evaluated using Eq. (11). This is because the mass fraction of dry substance of a saturated solution is only temperature-dependent. Then, the mass fraction of dry substance can be used in Eq. (10) for the sugar–water mass ratio.

The surface reaction mass transfer coefficient can be calculated using the equation:

$$k_r = k_{r0}\exp\left(-\frac{E}{RT}\right) \tag{12}$$

The diffusion mass transfer coefficient can be obtained from the Frössling equation [11]:

$$k_d = \left(Sh_0 + a\left(\frac{\rho_{ml}v d_c}{\eta_{ml}}\right)^b\left(\frac{\eta_{ml}}{\rho_{ml}D}\right)^{1/3}\right)\frac{D}{d_c} \tag{13}$$

The connection between spherical equivalent diameter and characteristic crystal size can be expressed by the equation:

$$\bar{L}_i = d_c\left(\frac{\pi}{6k_v}\right)^{0.33} \tag{14}$$

The relative velocity is calculated by the hindered settling equation:

$$v = \frac{K_1(\rho_{cr}-\rho_{ml})g\bar{L}_i^2(1-x_{cr})^{K_2}}{\eta_{ml}} \tag{15}$$

The required volume fraction of crystals in the hindered settling equation is obtained from the mass fraction of crystals when the density of crystals and that of mother liquid, as well as the mass fraction of crystals, are known.

$$x_{cr} = \frac{w_{cr}/\rho_{cr}}{(w_{cr}/\rho_{cr} + (1-w_{cr})/\rho_{ml})} \tag{16}$$

2.2.3. Definition equations

The initial mass fraction of crystals is calculated from the mass flows of crystals and mother liquor into the crystallizer:

$$w_{cr}(0) = \dot{m}_{cr}(0)/(\dot{m}_{cr}(0) + \dot{m}_{ml}(0)) \tag{17}$$

The total solid phase concentration in the beginning is calculated using equation:

$$M_{t0} = \dot{m}_{cr}(0)/(\dot{m}_{tot}/\rho_{ms}) \tag{18}$$

The linear flow velocity down the crystallizer can be calculated using equation:

$$v = \frac{\dot{m}_{tot}}{\rho_{ms}A} \tag{19}$$

Therefore, the linear velocity for the particles of size $\bar{L}_i$ can be calculated using the equation:

$$v_i = v + v_{set,i} \tag{20}$$

For a balance volume, $V = \Delta h(\pi D_T^2)/(4)$, the residence time of particles in size class i can be calculated using the following equation:

$$\tau_i = \frac{\Delta h}{v_i} \tag{21}$$

2.2.4. Equations describing the characteristics of particulate system

Population densities in the beginning can be calculated in the following way. The distribution is assumed to be of Rosin–Rammler type. The Rosin–Rammler distribution function is commonly used for sucrose. It has two parameters: Rosin–Rammler size and exponent. The Rosin–Rammler size depends mainly on the mean size of the distribution, while the exponent determines how wide the distribution is. The definition equation for Rosin–Rammler cumulative mass distribution is:

$$W(L) = 1 - \exp\left(-\left(\frac{L}{L_{RR}}\right)^{\omega}\right) \tag{22}$$

The Rosin–Rammler exponent, ω, can be evaluated from the coefficient of variation through the equation of Pezzi and Maurandi [12]

$$\mathrm{CV} = 100\frac{\left[\ln(100/15.87)\right]^{1/\omega} - \left[\ln(100/84.13)\right]^{1/\omega}}{2(\ln(2))^{1/\omega}} \tag{23}$$

and the Rosin–Rammler size, L_{RR}, is related to the mean aperture, MA, through

$$MA = L_{RR}(\ln 2)^{1/\omega} \quad (24)$$

The model is now developed using discrete crystal size classes. Population densities can be calculated from the cumulative mass distribution by using the equation presented by Randolph and Larson [1], p. 15:

$$n_i = \frac{M_{t0}\left(\frac{dW(L)}{dL}\right)_i}{\rho_{cr} k_v L_i^3} \quad (25)$$

Now, for the Rosin–Rammler distribution, the population densities can be calculated using the equation obtained by an analytical derivation of the cumulative mass distribution function:

$$n_i = \frac{M_{t0}\frac{1}{L_{RR}^{\omega}}\omega L_i^{\omega-1}\exp\left(-\left(\frac{L_i}{L_{RR}}\right)^{\omega}\right)}{\rho_{cr} k_v L_i^3} \quad (26)$$

The number flow of crystals in a specified size class is calculated from the population densities with the following equation:

$$N_i = \frac{\dot{m}_{tot}}{\rho_{ms}}\int_{L_{min,i}}^{L_{max,i}} n(L)\,dL \quad (27)$$

The characteristic size of a size class is defined by the equation:

$$\bar{L}_i = \frac{L_{max,i} + L_{min,i}}{2} \quad (28)$$

The initial mass flow of crystals in a specified size class can be expressed by the equation:

$$\dot{m}_{cr,i}(0) = N_i\,\rho_{cr} k_v \left(\bar{L}_i(0)\right)^3 \quad (29)$$

The average crystal size in the size class after a step j will be:

$$\bar{L}_i(j) = \bar{L}_i(j-1) + \bar{G}_i(j)\tau_i(j) \quad (30)$$

Nucleation and crystal breakage were assumed not to take place. Thus, the number flow of particles in any size class remains constant. The mass flow of crystals of a specified size class after step j is calculated using the equation:

$$\dot{m}_{cr,i}(j) = \dot{m}_{cr,i}(0)\left(\frac{\bar{L}_i(j)}{\bar{L}_i(0)}\right)^3 \quad (31)$$

The growth rates were, as previously mentioned, first calculated using the initial values of temperature, mass fraction of dry substance and mass fraction of crystals. Later, they were recalculated using the average values of these variables.

3. Use of the model for simulation

3.1. Input variables

The input variables for the simulation model were the following:

- Diameter of the tower D_t [m]: numerical values shown in the pictures
- Length of the tower h [m]: numerical values shown in the pictures
- Supersaturation ratio as a function of location S [ ]: assumed constant in simulations
- Feed information: numerical values shown in the pictures
  - Mass flow of the feed crystals $\dot{m}_{cr}$ [kg/s]
  - Mass flow of the feed mother liquor $\dot{m}_{ml}$ [kg/s]
  - Initial mass fraction of the dry substance w_{ds} [ ]
- Growth rate parameters
  - Diffusion parameters (taken from Heffels and de Jong [11])
    - Factor a [ ]
    - Reynolds number exponent b [ ]
  - Surface reaction parameters (taken from Austmeyer [13])
  - Arrhenius law factor $k_{r,0}$ [m/s]
  - Activation energy E [J/mol]
- Size ranges, which were calculated from the following variables:
  - Number of size classes N_{tot} [ ]
  - Minimum size L_{min} [m]
- Maximum size L_{max} [m]

The minimum size was selected so that, practically, the smallest crystal of the initial distribution was included. The maximum size was selected so that, practically, the largest crystal of the product was included. The number of size ranges was large enough to guarantee that the discretization error was small. Fifty size classes were used.

- Shape factors (numerical values from Heffels and de Jong [11])
  - Volume shape factor k_v [ ]
  - Area shape factor k_a [ ]
- Rosin–Rammler initial distribution parameters (calculated from the coefficient of variation and crystal mean size)
  - Rosin–Rammler exponent ω [ ]
  - Rosin–Rammler size L_{RR} [m]

The parameters of the initial distribution were obtained from known CV and MA typical for sugar, according to Eqs. (23) and (24).

3.2. Calculation strategy

The model is based on the idea that the crystallizer is divided into small sections inside, which the growth rate is assumed to be constant. The residence time of the particles is calculated based on their flow due to total mass flow and settling. When the growth rates for particles and their residence times are known, the sizes of the particles after the section can be calculated. Firstly, the growth rates and residence times are calculated assuming that conditions within the sections are identical to those of the entrance of the sections. This means that the mass fraction of the dry substance and crystals and temperature is assumed to be constant within the section. Later, after calculating the mass growth of crystals inside the step, these values are corrected to average values inside the step.

The calculation starts from the top with initial values for temperature, mass flow of crystals, CSD, mass flow of mother liquor and mass fraction of sugar in mother liquor. The target end temperature, the tower size and the constant supersaturation are fixed. Therefore, the total mass feed to the tower is iteratively adjusted to meet these specifications. The mass fraction of crystals is calculated with Eq. (17). The total solid phase concentration in the beginning is then obtained from Eq. (18). The linear flow velocity is calculated by dividing the known total volume flow by the cross section area according to Eq. (19). The settling velocity is calculated with Eq. (5) for all crystal sizes with required volume fraction of crystals from Eq. (16). The physical properties in Eq. (5) were known as a function of temperature and mass fraction of dry substance in mother liquor. The CSD on top was assumed to be of Rosin–Rammler form, Eq. (22). For the RR distribution, the population density is calculated with Eq. (26) for each selected size class. Thereafter, the number flow of crystals in each specified size class is obtained by integration according to Eq. (27). The initial mass flow of crystals in a specified size class is calculated from the known number and characteristic crystal size according to Eq. (29). In a section, the crystal size will increase according to the growth expression, Eqs. (8) and (9). In order to calculate the individual growth rates of crystals of various sizes, the mass transfer coefficients of both diffusion and surface reaction are required. These are obtained from Eqs. (12) and (13). The concentration difference between supersaturated and saturated solution is calculated by Eq. (10). The characteristic crystal sizes after each step are calculated from the known sizes before the step and the known growth rates in the step and from residence times according to Eq. (30). The required residence times are calculated from the known step length and linear velocities according to Eq. (21). The growth of crystals causes changes in the mass flow of the mother liquor and the mass fraction of dry substance in the mother liquor. The mass flow of mother liquor after the step is calculated from the known total mass flow and from the mass flow of crystals after the step according to Eq. (3). The mass fraction of dry substance after the step is calculated with the dry substance balance of Eq. (4). This also provides the temperature, which corresponds to the fixed supersaturation, when the solubility dependence on temperature is known. The calculation continues with similar reasoning step by step until the bottom of the column is reached.

The verification strategy included an experimental study of settling of sugar crystals and an order of magnitude study to confirm sucrose crystal growth. The tower crystallizer model has not yet been verified experimentally.

The program was written in the MODEST software using FORTRAN code. The computation was straightforward. The iterations were all solved with the secant method. No convergence difficulties were encountered. The simulation was made on an ordinary PC with a Pentium II processor.

3.3. Simulation case studies

Because of well-known material properties, sucrose was used as a model material in the simulation examples. However, the model is valid for other materials as well.

The following variable values were used in the simulation case studies:

Run number	1	2
Tower height [m]	20	20
Tower diameter [m]	4	4
Top/end temperature [°C]	70/20	70/20
Supersaturation coefficient	1.05	1.05
Initial yield	1%	20%
Initial average size [μm]	150	450
Final average size [μm] (calculation result, roughly)	500	500
Final yield (calculation result, roughly)	40%	60%

The mass flows were iterated so as to get the temperature in the tower down to 20°C. The model did not include energy balances. Appropriate cooling was assumed to take place and the temperature profile in the tower was calculated to correspond to a constant supersaturation value.

The narrowing of the CSD as a result of the settling phenomenon did not emerge, due to slow settling rates of small particles. Therefore, a new simulation with larger particles was attempted. The simulation results are presented in Figs. 2–7 for the first and Figs. 8–13 for the second case.

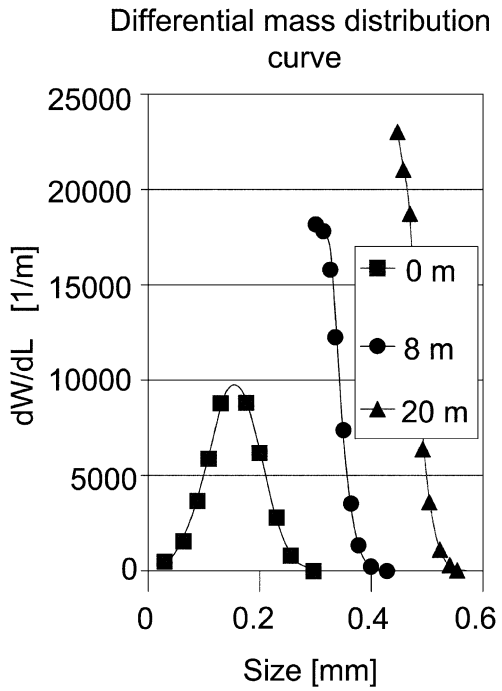

Fig. 2. Differential mass distribution for the first simulation case.

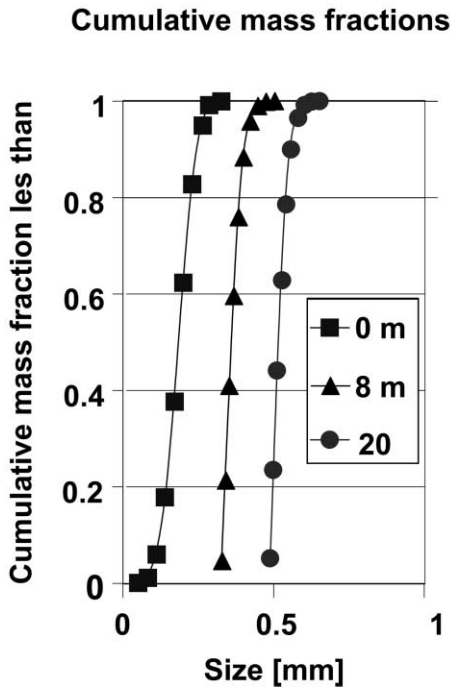

Fig. 4. Flow velocity and settling velocities for the first simulation case.

The main differences between the two studied cases were the initial crystal content and the initial mean crystal size.

4. Discussion of results and conclusions

Fig. 2 presents differential mass distribution curves for three locations, at the top in the middle and at the bottom of the column. A slight narrowing of the distribution can be seen. This was mainly due to the size-dependent growth expression.

Fig. 3 presents the total linear flow velocity and the settling rates of particles for selected size classes. The total flow velocity was at least an order of magnitude larger than the settling velocities. The total number of size classes was 50. The increase of settling velocities in the higher

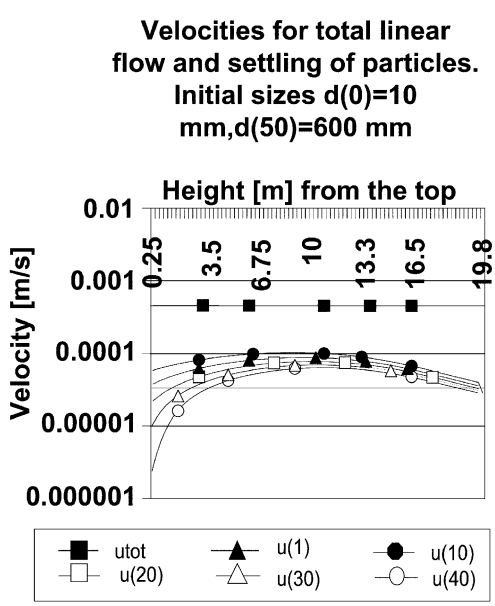

Fig. 3. Flow velocity and settling velocities for the first simulation case.

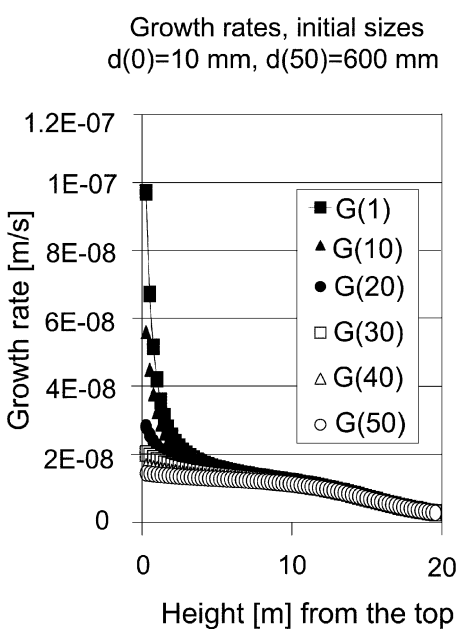

Fig. 5. Cumulative mass distribution for the first simulation case.

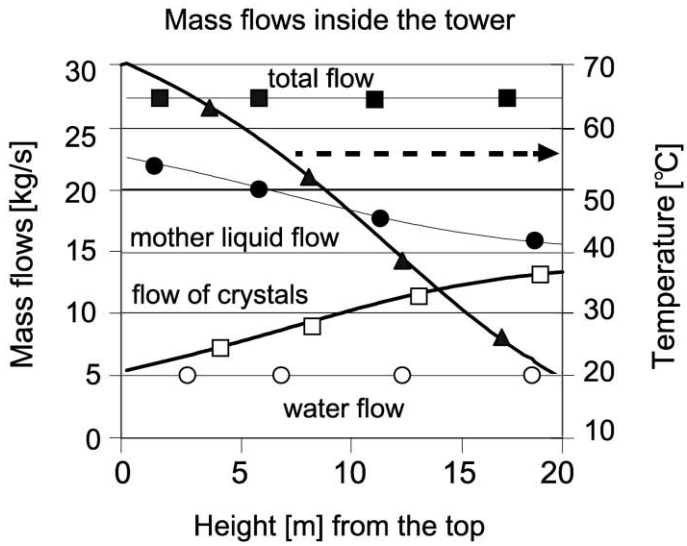

Fig. 6. Growth rates for the first simulation case.

part of the tower is due to size growth of the crystals, but in the lower parts, the increasing viscosity reverses this trend.

In Fig. 4, the cumulative mass distributions are presented at three locations in the tower. These curves show the change in the slopes indicating some narrowing. If growth rate dispersion had been included in the model, the narrowing of the CSD would probably be imperceptible or even reversed.

In Fig. 5, the growth rates are presented for the selected six size classes. From these curves, the size dependency of growth can be clearly seen. For very small crystals, the growth model estimated a strong growth. The growth was also a function of temperature, and the figure illustrates how the growth rate decreased remarkably as temperature decreased.

Fig. 6 illustrates mass flow and temperature profiles in the tower. The temperature profile is nonlinear from 70°C to 20°C. This is the consequence of constant supersaturation and the third power dependency of mass increase on crystal size. The mass flow of crystals increases due to the third power dependency of crystal mass on crystal size. Also, the temperature effect can be seen from the curve. The water flow and the total mass flow are constant, as they should. The decrease in mother liquor flow mirrors the increase of flow of crystal mass reflecting the sugar balance.

In Fig. 7, the mass fraction of crystals in the slurry and the mass fraction of dry substance in the mother liquor are presented. The form of the curve for the crystal mass fraction resembles the curve for the flow of crystals. Both the effect of the third power dependency of crystal mass on crystal size and the effect of temperature can be seen.

A similar set of figures is presented for the second simulation. Here, the initial crystal size as well as the initial crystal content was much larger. The relative in-

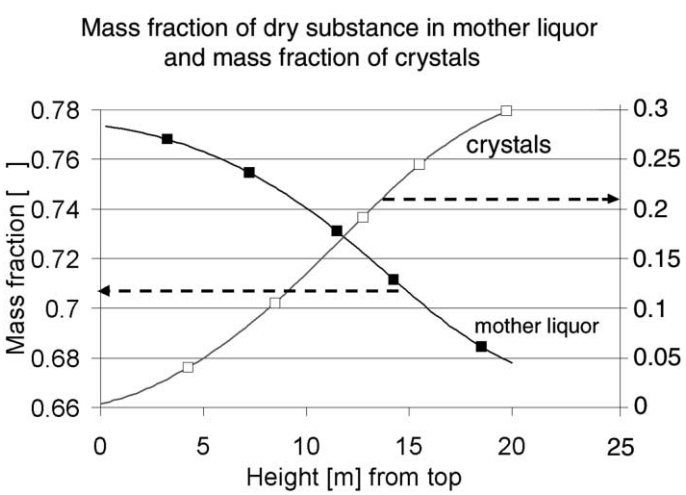

Fig. 7. Mass flows for the first simulation case.

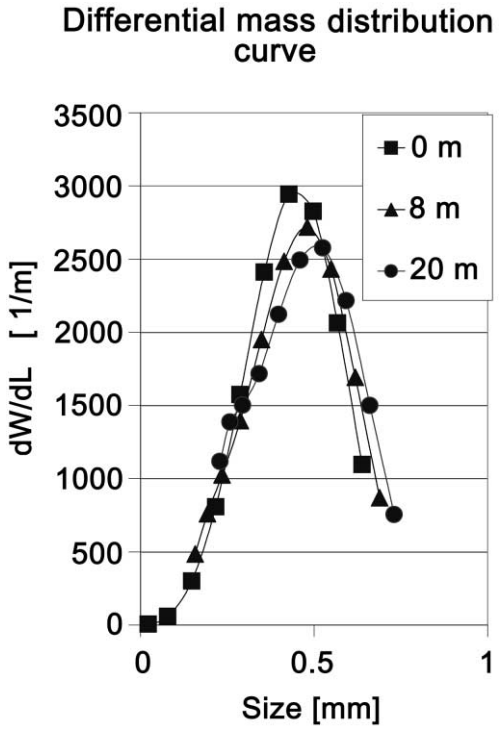

Fig. 8. Mass fractions for the second simulation case.

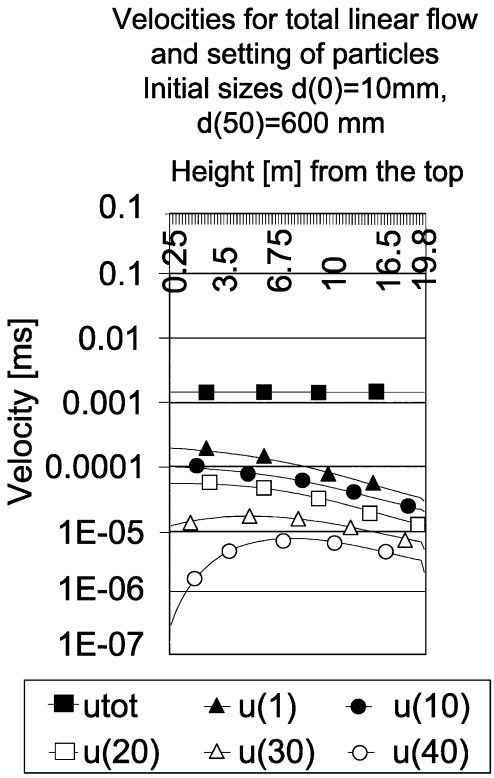

Fig. 10. Flow velocity and settling velocities for the second simulation case.

crease of crystal size was modest, which can be seen in the differential mass distribution curve (Fig. 8) and in the cumulative mass distribution curve (Fig. 9). The distribution curves did neither indicate a narrowing nor a broadening of the CSD. This may be due to the fact that the relative size increase was small. The settling velocities presented in Fig. 10 were again smaller than the total flow velocity. In Fig. 11, the growth rates for the largest size

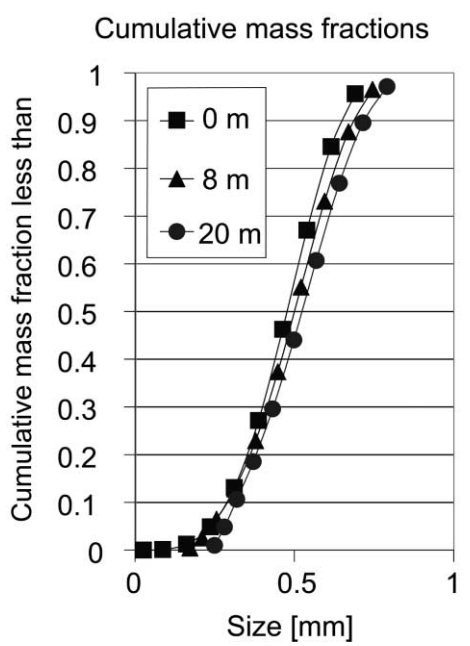

Fig. 9. Differential mass distribution for the second simulation case.

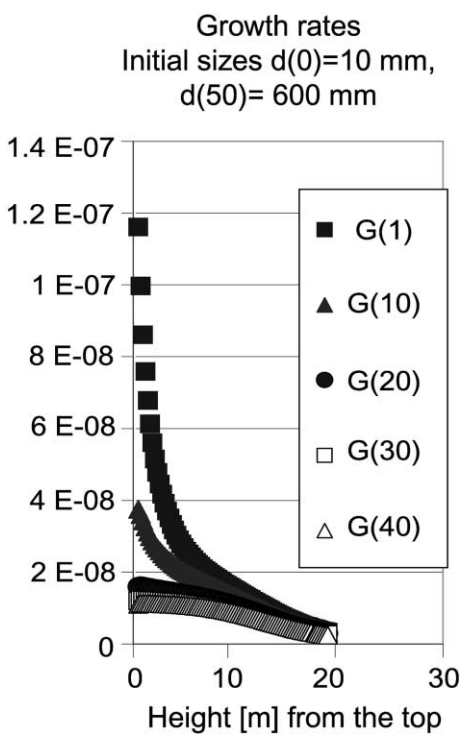

Fig. 11. Cumulative mass distribution for the second simulation case.

ranges were smaller because this time, the initial sizes were larger. The mass flow curves and the temperature curve presented in Fig. 12 were qualitatively similar to those of the first simulation case. That also holds for the mass fraction curve in Fig. 13.

The model estimated very small retention times for the sucrose cases. The settling velocities for small sucrose particles are so low that the phenomenon does not have any practical effect on CSD in that particle size range. The settling velocities, as described by the modified Stokes' hindered settling equation, are very strongly dependent on crystal size. This size dependency is of the second power of crystal size. Therefore, the narrowing of CSD should be seen more clearly with larger particles.

This fact was tested in simulation with larger sugar crystals. The settling velocities were observed to be in the same order of magnitude as the total flow. However, with larger crystal sizes, the relative change of crystal sizes was smaller. Therefore, the effect of settling could not be seen so clearly.

For pure sucrose, the settling may have an effect on crystallization only when large crystals are involved. For impure sucrose solution, the growth rates are much slower, but, also, the settling velocities are slower due to higher viscosity. Therefore, only simulations with proper growth expressions and settling equations for that particular case may give evidence of settling affecting the CSD.

Growth rate expression was the one taken from literature and it indicated a strong size dependency of growth due to mass transfer. Since this equation gave larger growth rates for smaller particles, it caused some narrowing of the CSD. For very small sucrose crystals (size less than 100 μm), the growth rates are not well-known and, therefore, the results in that size range are unsure.

Mass flow of crystals increases more rapidly in the upper part of the tower. This is because growth is temperature- and size-dependent. The growth slows down as temperature decreases.

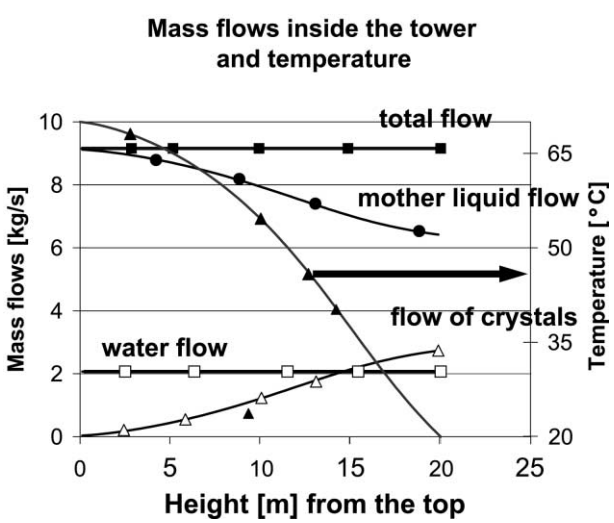

Fig. 12. Growth rates for the second simulation case.

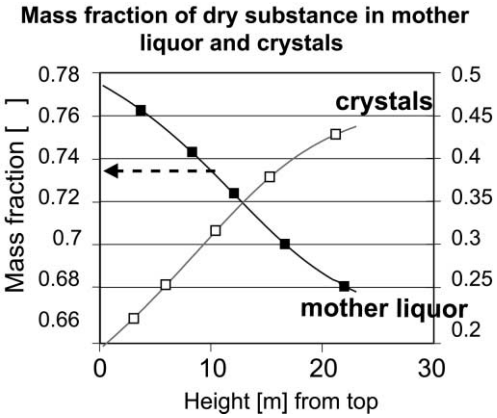

Fig. 13. Mass flows for the second simulation case.

Temperature trend curves are nonlinear as expected. The supersaturation was constant inside the tower, and this mainly caused the nonlinear behaviour. Constant supersaturation is an optimal way to run the crystallization and, therefore, it was used in all the simulations. The now obtained cooling curves resemble qualitatively the constant supersaturation cooling curves of batch crystallization.

List of variables

A	cross sectional area of the crystallizer [m^2]
A_c	total surface area of crystals [m^2] in Eqs. (6) and (8)
a, b	diffusion growth rate parameters
CV	coefficient of variation [%]
D	diffusivity [m^2/s]
d_c	spherical equivalent diameter of particles [m]
D_T	diameter of the crystallizer [m]
$(dW(L)/dL)i$	derivative of cumulative mass distribution at size L_i [1/m]
E	activation energy [J/mol]
g	gravity constant [m/s^2]
G	growth rate [m/s]
$\overline{G}_i(j)$	average growth rate of the ith size class in step j [m/s]
h	height of the tower [m]
K_1, K_2	coefficients in settling equation
k_a	area shape factor
k_d	mass transfer coefficient for diffusion [m/s]
K_g	overall mass transfer coefficient [m/s]
k_r	mass transfer coefficient for surface reaction [m/s]
k_{r0}	Arrhenius law factor [m/s]
k_v	volume shape factor
L	crystal size [m]
$\overline{L}_i$	average size of crystals in the size class i [m]
$\overline{L}_i(0)$	inlet average size of crystals in the size class i [m]
$\overline{L}_i(j)$	average size of the ith size class after step j [m]
$\overline{L}_i(j-1)$	average size of the ith size class after step $j-1$ [m]

$L_{max,i}$ maximum size in the size class i [m]
$L_{min,i}$ minimum size in the size class i [m]
L_{RR} Rosin–Rammler size [m]
MA mean aperture [m]
$\dot{m}_{cr}(0)$ inlet mass flow of crystals in feed [kg/s]
$\dot{m}_{cr,i}(0)$ inlet mass flow of crystals in the size class i [kg/s]
$\dot{m}_{cr,i}(j)$ mass flow of crystals of the ith size class after the jth step [kg/s]
$\dot{m}_{ml}(0)$ inlet mass flow of mother liquor in feed [kg/s]
$\dot{m}_{ml}(j)$ mass flow of mother liquor after the jth step [kg/s]
M_{t0} inlet total solid phase concentration [kg crystals/m^3 of mass]
$\dot{m}_{tot}$ total mass flow [kg/s]
N_i number flow of particles in the size class [1/s]
n_i population density of crystals of size L_i [1/m^4]
$n(L)$ population density as a function of size [1/m^4]
N_s total number of size classes
$q_{s/w}$ sugar water mass ratio
$q_{s/w,sat}$ sugar water ratio of saturated solution
R general gas constant [J/(mol K)]
S supersaturation coefficient
Sh_0 Sherwood number for zero flow
t time [s]
T absolute temperature [K]
T_0 temperature on top of the crystallizer [K]
T_i temperature at the ith step [K]
$W(L)$ cumulative mass fraction
$w_{cr}(0)$ initial mass fraction of crystals
$w_{ds}(0)$ initial mass fraction of dry substance
$w_{ds}(j)$ mass fraction of dry substance in mother liquor after the jth step
$w_{ds,sat}$ saturation mass fraction of dry substance
v linear total flow velocity [m/s]
v_i linear flow velocity of particles of average size $\bar{L}_i$ [m/s]
$v_{set,i}$ settling velocity of crystals of size $\bar{L}_i$ [m]
x_{cr} volume fraction of crystals
ΔC concentration difference between supersaturated and saturated solution [kg/m^3]
Δh vertical step length [m]
ω Rosin–Rammler exponent
ρ_{cr} density of crystals [kg/m^3]
ρ_{sat} density of saturated solution [kg/m^3]
ρ_{ms} density of total mass [kg/m^3]
ρ_{ml} density of mother liquid [kg/m^3]
η_{ml} viscosity of mother liquid [kg/(ms)]
τ_i residence time in the balance volume [s]

References

[1] A. Randolph, M. Larson, Theory of Particulate Processes, Academic Press, San Diego, 1988.
[2] A. Myerson, Handbook of Industrial Crystallization, Butterworth-Heinemann Series in Chemical Engineering, 1993 USA.
[3] A. Mersmann, Crystallization Technology Handbook, Marcel Dekker, New York, 1995.
[4] N. Tavare, Industrial Crystallization, Plenum, New York, 1995.
[5] K. Ramarao, K. Venkataratnam, O. Reddy, Preliminary trials of continuous crystallizers, 43rd Annual Convention of Sugar Technology Association of India, October 1979, Kanpur, 1979.
[6] H. Dunker, Die Nachproductarbeit mit Vertikalmaischen in der Zuckerfabrik Süderdithmarschen AG, St Michaelisdonn, Zuckerindustrie 107 (4) (1982) 296–301.
[7] M.A. Sima, J. Harris, Modelling of a low grade vertical cooling crystallizer using computational fluid dynamics, Proceedings of Australian Society of Sugar Cane Technologists, 1997.
[8] P. Ditl, L. Beranek, F. Rieger, Simulation of a stirred sugar boiling pan, Zuckerindustrie 115 (8) (1990) 667–676.
[9] B. Ekelhof, Gesamtmodell der Kristallisationskinetik der Saccharose in reinen und unreinen Lösungen, Bartens, Berlin, Germany, 1997.
[10] Z. Bubnik, P. Kadlec, D. Urban, M. Bruhns, Sugar Technologist's Manual, Bartens, Berlin, Germany, 1995.
[11] S. Heffels, E. de Jong, Modelling sucrose crystal growth, Zuckerindustrie 113 (9) (1988) 781–786.
[12] G. Pezzi, V. Maurandi, Numerical methods for calculations of sugar grain size distribution, Zuckerindustrie 118 (2) (1993) 113–123.